Research Article

Tao Yang#, Junhui Wang#, Jiali Tu, Xiaoxi Zhou, Jiamin Sun, Jian Chen, Wanxin Wen*, and Yanfei Wang*

Rare-earth doped radioluminescent hydrogel as a potential phantom material for 3D gel dosimeter

https://doi.org/10.1515/epoly-2021-0053
received May 05, 2021; accepted June 27, 2021

Abstract: Cancer prevention and treatment are currently the focus of most research. Dose verification is an important step for reducing the improper dose deposition during radiotherapy. To mend the traditional gel dosimeters for 3D dose verification, a novel rare-earth nanoparticle-based composite gel was prepared, which has good radioluminescence property and reusability. It is a promising phantom material for the new 3D gel dosimeter. TEM, DLS, FT-IR, TGA, and spectrofluorometer were used to determine the chemical structure, micromorphology, and optical performance. Compared to the traditional gel dosimeters, the composite gel has a good linear relationship between the light intensity excited by X-ray and the tube current. Furthermore, it may measure the dose distribution immediately *in situ*, which reduces errors and saves time. This work provides a new idea for the research of 3D gel dosimeters and promotes the safe and effective use of radiotherapy.

Keywords: rare-earth nanoparticles, radioluminescence, composite gel, dose verification, gel dosimeter

1 Introduction

In 2020, there were approximately 1.93 million new cancer patients and 10.0 million deaths due to cancer worldwide (1), leading to more attention in cancer prevention and treatment. Depending on the stage and type of cancer, about 50–65% of all cancer patients need radiotherapy, which may kill both cancer cells and normal cells and cause damage to normal tissues and organs (2). Dose verification is a key step for reducing improper dose deposition. Currently, 3D dose verification is one of the important research topics for future dose verification.

Gel dosimeter has been investigated since 1950 and it has been applied in clinics (3,4). However, these traditional gel dosimeters still have some drawbacks. For instance, a main limitation of the Fricke gel dosimeter is the diffusion of the ferrous and ferric ions following irradiation that may affect the result of dose distribution measurement (5). Polymeric gel dosimeter has a long polymerization time, which takes more than 48 h (6), and therefore, this kind of dosimeter is inefficient. The radiochromic gel dosimeter has poor transparency, which disturbs the follow-up measurement of light absorption. In view of this, many studies have been focused on improving these gel dosimeters in recent years. Zhang et al. developed a novel Fricke gel dosimeter that featured a low diffusion of Fe^{3+} by virtue of $W_1/O/W_2$ emulsion (7). The Lazzaroni group also reported a new Fricke dosimeter with a selective ligand for overcoming several limitations (8). Zin et al. prepared a new MAGAT dosimeter (polymeric gel dosimeter) with the addition of methylene blue and zinc oxide. The results showed that methylene blue reduced self-polymerization and zinc oxide increased the dose response (9). The Kenichi Tanaka group synthesized a novel radiochromic gel dosimeter by the complexation of polyvinyl alcohol and

# These authors contributed equally.

*** Corresponding author: Wanxin Wen,** State Key Laboratory of Radiation Medicine and Protection, Soochow University, Suzhou 215123, China; Research Center of Multimoding Radiation Technology, School of Radiation Medicine and Protection, Soochow University, Suzhou 215123, China, e-mail: wxwen@suda.edu.cn
*** Corresponding author: Yanfei Wang,** Department of Radiotherapy, Affiliated Hospital of Nantong University, Nantong 226001, China; Department of Medical Ultrasound, Affiliated Hospital of Nantong University, Nantong 226001, China, e-mail: ratec@foxmail.com
Tao Yang: Department of Radiotherapy, Affiliated Hospital of Nantong University, Nantong 226001, China; Research Center of Multimoding Radiation Technology, School of Radiation Medicine and Protection, Soochow University, Suzhou 215123, China
Junhui Wang: Department of Radiotherapy, Nantong Tumor Hospital, Nantong 226362, China
Jiali Tu, Xiaoxi Zhou, Jiamin Sun, Jian Chen: Department of Radiotherapy, Affiliated Hospital of Nantong University, Nantong 226001, China

iodide, which exhibited reusability, high sensitivity, and transparency (10). Recently, radio-fluorogenic gel dosimeters have been expected to become new dose distribution measurement tools. Watanabe et al. developed a nanoclay-based radio-fluorogenic gel (NC-RFG) dosimeter using dihydrorhodamine 123 hydrochloride as a fluorescent probe to measure the dose distribution and demonstrated that this NC-RFG had the potential of being a useful tool for dose verification delivered by high-dose-rate brachytherapy (11). The Warman's group reported a radio-fluorogenic polymer gel with gamma-ray-polymerized tertiary-butyl acrylate and maleimido-pyrene (fluorogenic compound), which also provided a method for 3D dosimetry (12). Liang Hu's group designed a nanogel sensor by anchoring aminophenyl fluorescein to poly(acrylamide-*co*-*N*-(3-aminopropyl)methylacrylamide) nanogels (13). These dose measurements employed radioluminescent signal indirectly, which may lead to a potential increase in the probability of error.

In this research, a novel radioluminescent composite gel for a 3D gel dosimeter was synthesized via photoinitiated polymerization. This reusable gel material is composed of a hydrogel (polyacrylamide gel, as a matrix) and rare earth nanoparticles (Gd_2O_2S:Eu, as a radiation responsive probe). The dose distribution can be measured *in situ*, which may reduce error and save time.

2 Materials and methods

2.1 Materials

Gadolinium chloride hexahydrate ($GdCl_3{\cdot}6H_2O$), europium chloride hexahydrate ($EuCl_3{\cdot}6H_2O$), 2-hydroxy-4′-(2-hydroxyethoxy)-2-methylpropiophenone (Irgacure 2959), sodium diethyldithiocarbamate trihydrate (Na(ddtc)·$3H_2O$), oleylamine, 1-octadecene, and 1,10-phenanthroline ($C_{12}H_8N_2$) were purchased from Aladdin Reagent (Shanghai, China). Cyclohexane, chloroform, acrylamide (AAm), *N*,*N*′-methylenebisacrylamide (BIS), acetone, and absolute ethanol were purchased from Sinopharm Chemical Reagent (Shanghai, China). Oleic acid was obtained from Macklin Biochemical (Shanghai, China). DSPE-PEG_{5k}-Mal was bought from Yare Biotech (Shanghai, China). All chemicals were used as received without further purification. Nitrogen was obtained from Jinhong Gas (Suzhou, China). Deionized (DI) water was produced by a Milli-Q Plus system (USA).

2.2 Preparation of Gd_2O_2S:Eu nanoparticles

Synthesis of precursor $Gd(ddtc)_3(Phen)$: in a 3-neck round bottom flask, Phen·H_2O (1 mmol, 40 mL) solution was stirred and heated to 100°C to which was added a solution of $GdCl_3{\cdot}6H_2O$ (1 mmol, 20 mL) under vigorous stirring. After that, Na(Dalkdtc)·H_2O (3 mmol, 40 mL) solution was added dropwise to the flask under constant stirring for 2 h. After the reaction, the precipitate was washed several times and dried in a vacuum for further use (14,15).

Synthesis of precursor $Eu(ddtc)_3(Phen)$: the three raw materials, $EuCl_3{\cdot}6H_2O$ (1 mmol, 10 mL), Phen·H_2O (1 mmol, 40 mL), and Na(Dalkdtc)·H_2O (3 mmol, 20 mL) were used. The synthesis procedure was the same as $Gd(ddtc)_3(Phen)$.

The Gd_2O_2S:Eu nanoparticles (the patterns match well with the standard Gd_2O_2S reflection, JCPDS No. 026-1422) were synthesized via a typical method with slight modification (16–18). In a typical procedure, 0.5 g of $Gd(ddtc)_3(Phen)$ and 0.05 g of $Eu(ddtc)_3(Phen)$ were added to a mixed solution of oleylamine (30 mmol, 9.84 mL), oleic acid (5 mmol, 1.6 mL), and 1-octadecene (30 mmol, 7.58 g) at room temperature under constant stirring. To remove air, nitrogen was continuously pumped into the 3-neck round bottom flask. The mixture was heated to 120°C and kept for about 30 min until a homogeneous, clear greenish-yellow solution was formed. Then, the nitrogen flow was stopped and the solution was rapidly heated to 290°C, over 5 min and kept for 2 h under constant stirring. The solution was cooled to room temperature and the Gd_2O_2S:Eu nanoparticles were precipitated by adding excess precipitant (hexane/acetone, 1:5). Then, the nanoparticles were washed and dried in a vacuum oven at room temperature for further use.

2.3 Modification of hydrophobic Gd_2O_2S:Eu nanoparticles

About 100 mg of DSPE-PEG_{5k}-Mal was added to 10 mL of chloroform to which was added 20 mg of Gd_2O_2S:Eu in 5 mL chloroform with ultrasonication. After stirring for 6 h at room temperature, the chloroform was evaporated by pumping nitrogen. Then, the residue was re-dispersed in 5 mL of DI water with the aid of sonication for 30 min. The resulting solution was filtered through a 0.2 µm membrane filter and water-dispersible Gd_2O_2S:Eu@PEG nanoparticles were obtained after centrifugation.

2.4 Synthesis of composite hydrogel

In a typical procedure, the precursor of composite hydrogel was obtained by mixing designated contents of AAm (0.4 g), BIS (0.8 mg), Gd_2O_2S:Eu@PEG (50 mg) and photoinitiator Irgacure 2959 (0.4 mg, relative to the concentration of AAm), and DI water (4 mL) in a glass vial with ultrasonication for 5 min to ensure homogeneous dispersion. After purging with nitrogen for 30 min, the vial was irradiated under 365 nm UV light (distance = 5 cm, intensity = 20 mW cm^{-2}) for 1 h.

3 Characterization

3.1 Transmission electron microscopy measurements

The morphology of nanoparticles was investigated by transmission electron microscopy (TEM, Tecnai F20, FEI, USA). The samples were diluted and then dripped on copper grids. Before TEM observation, the samples were dried at room temperature for 24 h and then heated under a mercury lamp for 15 min.

3.2 Particle size analysis

The hydrodynamic diameters of nanoparticles were determined by dynamic light scattering (DLS, Zetasizer Nano ZS90, Malvern, UK). The samples were dispersed in DI water and chloroform. Approximately 2 mL of the diluted solution after ultrasonication for 5 min was analyzed.

3.3 FT-IR spectra measurements

FT-IR spectra of the ground samples (Gd_2O_2S:Eu and Gd_2O_2S:Eu@PEG) were recorded on a Nicolet iS50 ATR FTIR spectrometer (Thermo Fisher Scientific, USA).

3.4 Thermal stability measurements

Thermogravimetric data were recorded on an SDT 2960 thermal gravimetric analyzer (TGA, TA Instruments, USA). The fully dried samples (5–10 mg) were added to an alumina crucible. The temperature range was 30–900°C and the samples were heated under a nitrogen atmosphere at a rate of 10°C min^{-1}.

3.5 Determination of luminescence property

The fluorescence emission spectra were obtained using an FLS 980 spectrofluorometer (Edinburgh Instruments, UK). Combined with the existing conditions of the laboratory, the Nova spectrometer (Fuxiang Optica, China) and the D8 Advance X-ray diffraction (Bruker, US) were used to measure the radioluminescence of the products. The ray energy (maximum energy is 40 kV) used in this experiment was kilovolt level radiation, which was different from the megavolt level radiation used in radiotherapy. The samples with a size of 1 cm^3 were placed on the specimen stage directly without any container. The measurement voltage of the D8 XRD was set to 40 kV, the current range was 15–40 mA, and the interval was 5 mA. The dose rates of different tube currents were 0.67, 0.89, 1.11, 1.33, 1.56, and 1.78 cGy. A rough estimation of the dose can be calculated based on the dose rate and measurement time. The probe was fixed in a suitable position of D8 XRD and connected to a Nova spectrometer (out of the D8 XRD) through an optical fiber. For reflection mode measurement, the integration time of the spectrometer was 5,000 ms, and the CCD cooling temperature was –20°C.

4 Results and discussion

4.1 Micromorphology of the nanoparticles

From the transmission electron microscopy (TEM) images and dynamic light scattering (DLS) data in Figures 1 and 2, neither obvious morphological change nor severe particle aggregation was observed, and the TEM images of Gd_2O_2S:Eu nanoparticles showed a platy structure with a hydrodynamic diameter of ~27 nm, which was smaller than that of Gd_2O_2S:Eu@PEG (~53 nm). These results intuitively indicated that the modification was successful.

4.2 FT-IR spectra

FT-IR spectroscopy was performed to verify the chemical composition of the products. Figure 3 illustrates the FT-IR

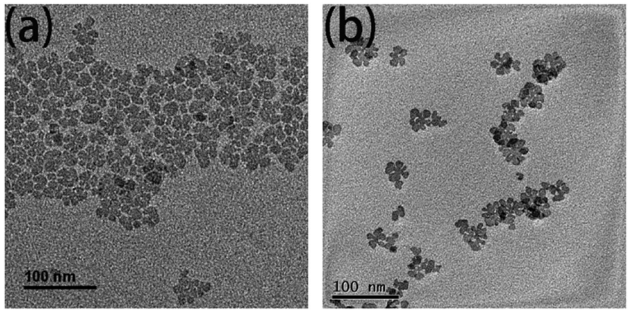

Figure 1: TEM images of Gd_2O_2S:Eu before (a) and after modification (b).

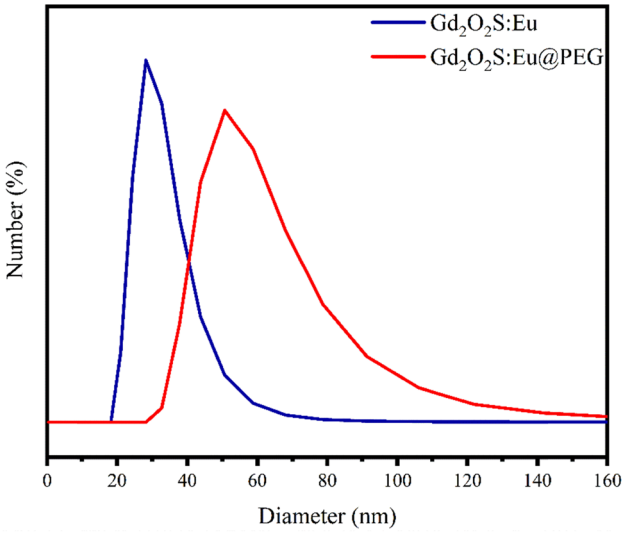

Figure 2: Particle size of Gd_2O_2S:Eu before and after modification measured by DLS.

spectra of Gd_2O_2S:Eu and Gd_2O_2S:Eu@PEG. The Gd_2O_2S:Eu nanoparticles showed characteristic peaks at 2,921 and 2,851 cm^{-1} that could be attributed to C–H stretching vibration; the absorption peaks at 1,596 and 1,420 cm^{-1} could be attributed to the N–H stretching vibration and COO^- symmetric stretching, respectively; and the absorption peaks at 1,072 cm^{-1} could be attributed to the C–N stretching vibration. These absorption peaks indicated that oleylamine and oleic acid were present in the unmodified nanoparticles as stabilizers (19). For Gd_2O_2S:Eu@PEG, the absorption peak at 1666.8 cm^{-1} belonging to the C═O stretching vibration almost disappeared; and the modified material also had a broad, weak band stretching at 3,200–3,500 cm^{-1}, attributed to N–H. These two peaks were characteristic absorption peaks of secondary amine groups in PEG (20). The absorption peaks at 2,881 and 962 cm^{-1} were attributed to the $-CH_2$ stretching vibration and the –CH out-of-plane bending vibration, respectively, and a strong absorption peak at 1,097 cm^{-1} could be ascribed to the C–O stretching vibration; these three peaks belong to PEG. The results of FT-IR spectra confirmed that the modification of Gd_2O_2S:Eu was successful in terms of chemical composition (21).

4.3 Thermogravimetric analysis

Figure 4 illustrates the TGA curves. For Gd_2O_2S:Eu, the residual weight percent of the sample was 66.5% and the curve could be divided into four main phases. The first phase occurred in the temperature range 100–350°C and was attributed to the decarboxylation of oleate groups. In

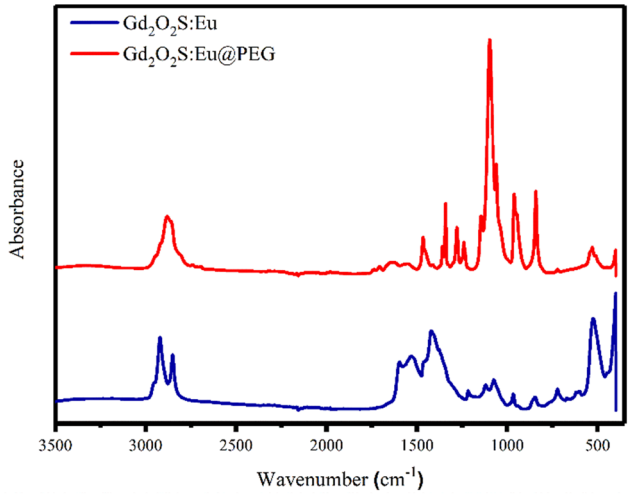

Figure 3: FT-IR spectra of Gd_2O_2S:Eu before and after modification.

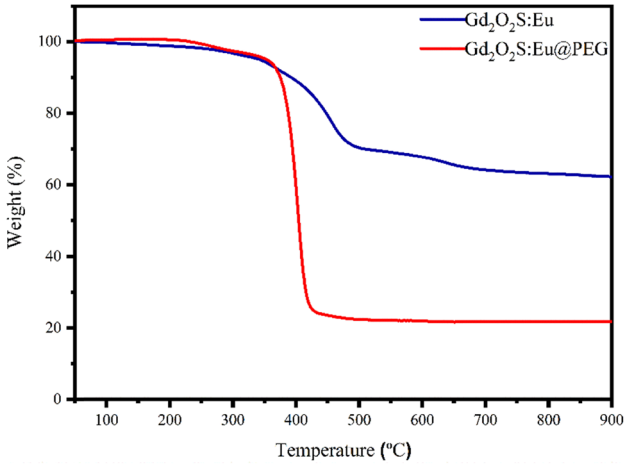

Figure 4: Thermogravimetric analysis of Gd_2O_2S:Eu before and after modification.

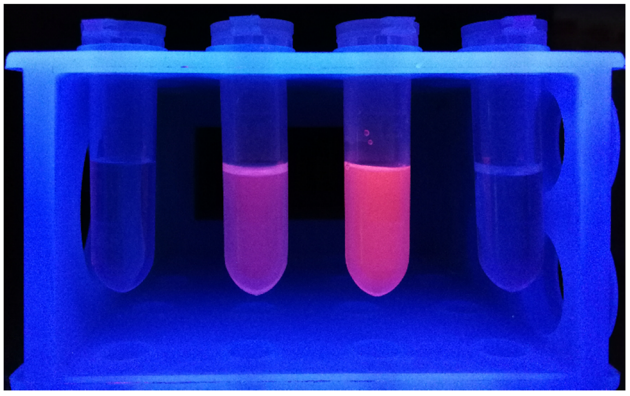

Figure 5: Photographs of water, Gd_2O_2S:Eu@PEG aqueous solution, Gd_2O_2S:Eu chloroform solution, and chloroform (under 254 nm UV).

the second phase (350–490°C), decomposition of the major part of organic-based ligands occurred, resulting in the major weight loss. In the third phase (490–720°C), the reaction between the free carbon and excess oxygen (formed by the decomposition of Gd_2O_2S) took place, which might produce CO_2 and CO (22). In the last phase (720–900°C), a slight weight loss was attributed to the removal of H_2S (formed by a limited degradation of the oxysulfide phase). For Gd_2O_2S:Eu@PEG, the total weight loss between 30°C and 900°C was 79.5%, corresponding to four-fifth of the sample that had been removed as volatile substances during the heating process. The major weight loss was observed in the temperature range of 370–430°C, and the main reason was the decomposition of a large amount of PEG. TGA analysis also indicated that the surface modification of nanoparticles was successful from another aspect.

4.4 Analysis of fluorescence property

As shown in Figure 5, the solutions of Gd_2O_2S:Eu and Gd_2O_2S:Eu@PEG were photographed under 254 nm UV

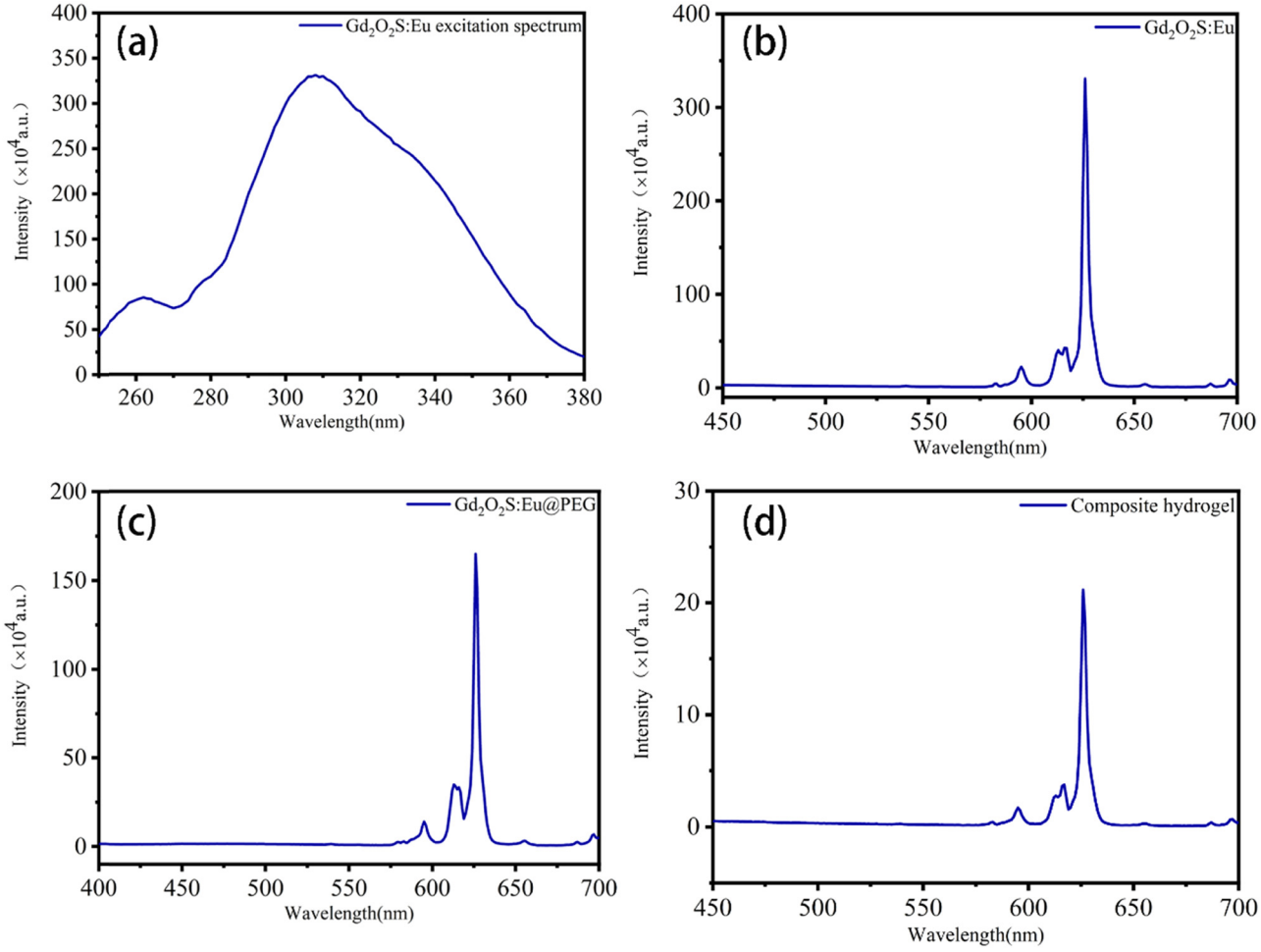

Figure 6: (a) Excitation spectra of Gd_2O_2S:Eu. (b–d) Emission spectra of Gd_2O_2S:Eu, Gd_2O_2S:Eu@PEG, and the composite gel (λ_{ex} = 310 nm).

light (tube 1, water; tube 4, chloroform). Both tube 2 and tube 3 are red, while the color is slightly lighter and the intensity is weaker of tube 2, which may result from the concentration and the optical quenching in water. The excitation spectrum has a wide range (200–400 nm), which is due to the charge transfer band between the anions and the Eu^{3+} ions. The excitation around 310 nm (Xe lamp as an excitation source) is attributed to the transition from the S^{2-} to Eu^{3+}, which may yield an ideal intensity of emission. Figure 6b–d shows the emission spectra of the Gd_2O_2S:Eu, Gd_2O_2S:Eu@PEG, and the composite hydrogel. The significant emission peaks are at about 625 nm (due to the forced electric-dipole $^5D_0 \rightarrow {}^7F_2$ transitions of the Eu^{3+}) (18), which is consistent with the results observed in the above photograph. From these results, it can be seen that the modification of nanoparticles or blending into gel does not change the fluorescence property. As shown in Figure 7, the composite hydrogel (right) and control sample were photographed under daylight lamp and 254 nm UV light. The composite gel (Figure 7d) is red and clearly indicates that Gd_2O_2S:Eu@PEG nanoparticles were successfully incorporated into the hydrogel.

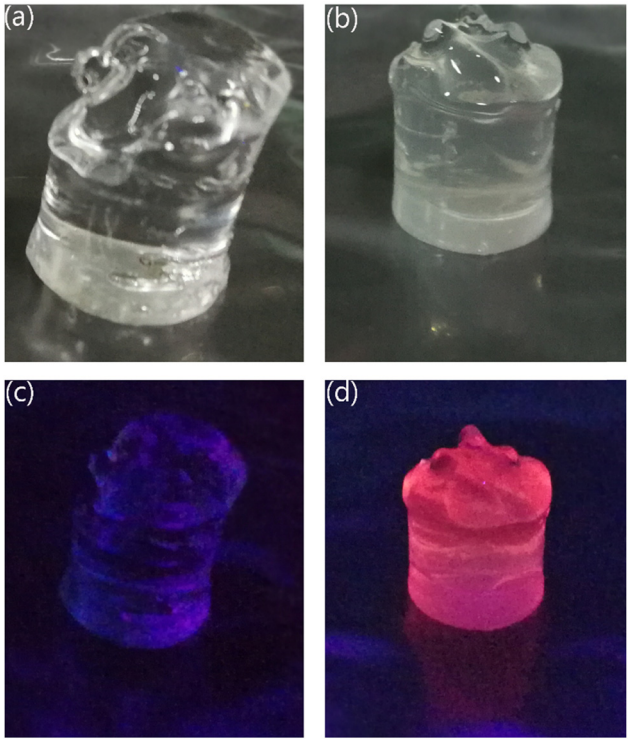

Figure 7: (a and b)Photographs of control sample (without Gd_2O_2S:Eu@PEG) and composite gel under daylight lamp. (c and d) Under 254 nm UV light.

4.5 Analysis of radioluminescence property

Figure 8 shows the emission spectrum of the composite gel excited by X-ray. The significant emission peak is located near 625 nm, and the result is consistent with that of the UV-excited emission peak. This may confirm that the composite gel has good radioluminescence properties.

Figure 9a shows the relationship between different tube currents and light intensity (excited by X-ray). This result indicates that the light intensity is proportional to the tube current when the tube voltage is constant. As shown in Figure 9b, the value of light intensity (Y) is proportional to the magnitude of the tube current (X) with good linearity ($R^2 = 0.9889$). Quantitatively, the light intensity can be determined as a function of the tube current of X-ray (Eq. 1):

$$Y = 0.2312 + 0.7799 \times X \quad (1)$$

This may demonstrate that the composite gel features a good linear response to the dose of X-ray.

4.6 Discussion

Gd_2O_2S:Eu particles were chosen because they emit red light (625 nm) with good penetration ability. Among the commonly used rare earth luminescent materials, Tb-doped nanomaterials also have radioluminescence properties and emit green light (550 nm) with weak penetrating ability. In order to facilitate the research and be limited by the experimental conditions, the composite gel synthesized in the experiment had a small size (see Figure 7). The next research direction is to adjust the

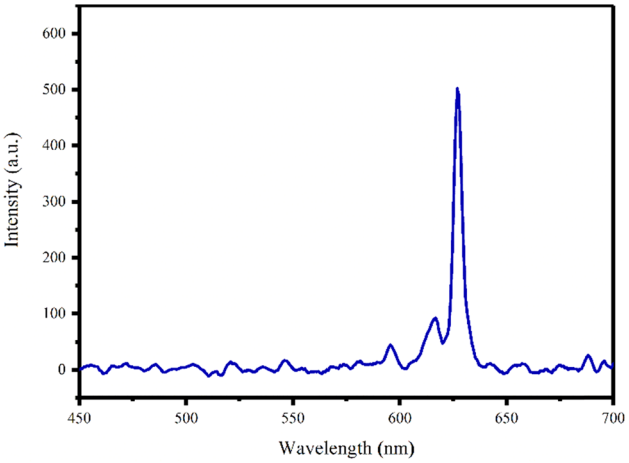

Figure 8: The emission spectrum of the composite gel excited by X-ray.

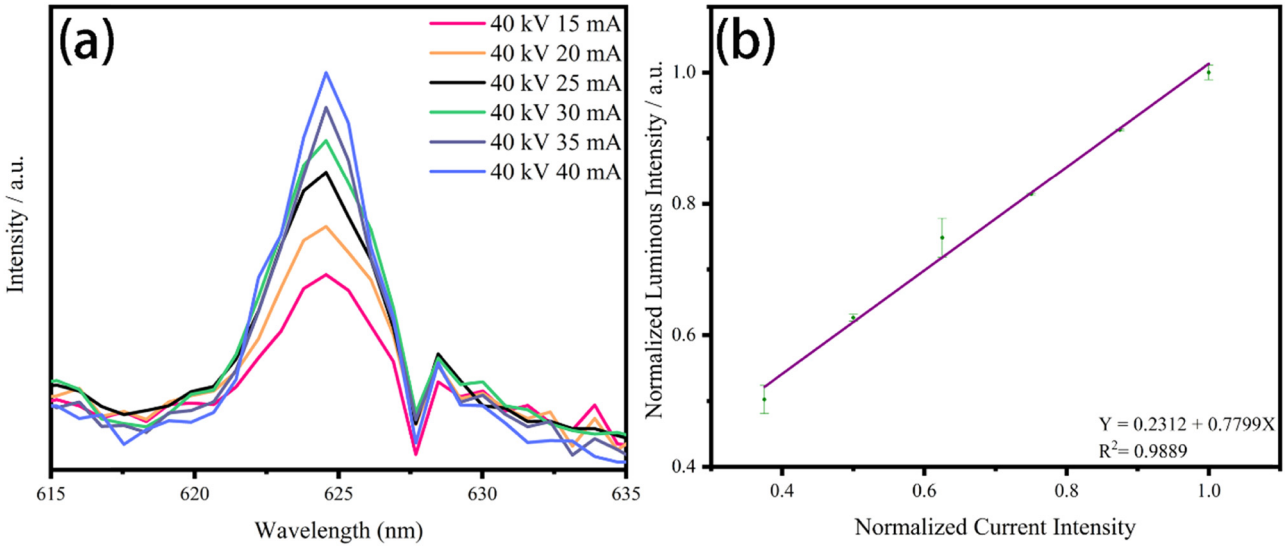

Figure 9: (a) The curves of light intensity with different tube currents and (b) the light intensity of the composite gel as a function of varying tube currents.

wavelength of the emitted light and to synthesize radioluminescent rare-earth nanomaterials, which can emit the second near-infrared (NIR-II) light. The NIR-II light has a wavelength ranging from 1,000 to 1,700 nm, which has the better penetrating ability and can reduce scattering and autofluorescence (23). The synthesis can be achieved by doping with Ln^{3+} (such as Yb^{3+}, Er^{3+}, Ho^{3+}, and Nd^{3+}).

In order to acquire the dose distribution information, the spatial and directional information of the optical signal from the composite gel can be recorded using a plenoptic camera (also called a light field camera). The Electronic Portal Imaging Device (EPID) integrated with linear accelerator can record the relative 2D beam's eye view (BEV) projection of the incident dose distribution easily. The 3D emitted light pattern of the composite gel may be reconstructed by spatial and angular information. Using an iterative reconstruction algorithm, the optical signal received by the camera can be back-projected to the composite gel. The 3D dose distribution can be acquired from the 3D light pattern, as the intensity of the optical signal is proportional to the energy deposited in the composite gel. The reconstruction model is as follows:

$$\vec{p} = A\vec{D} \tag{2}$$

where $\vec{p}$ is the given plenoptic projection and $\vec{D}$ is the relative emitted optical signal distribution discretized into voxels. "A" represents the system matrix that describes how the composite gel is imaged by the plenoptic camera. The constraints of Eq. 2 can be satisfied using the expectation-maximization algorithm and the reconstruction process is also constrained by the relative shape of the BEV dose projection and the depth in the composite gel (24).

Tissue equivalence and reusability: According to the above synthesis method, the mass of water in the composite gel accounts for 89.86% of the total mass. This conclusion is consistent with the water content in the BANG-1 polymer gel dosimeter (25). The reusability in this article is compared to the polymer gel dosimeter, Fricke gel dosemeter, and so on. Radioluminescence is an inherent property of the composite gel and it will not lose this property after irradiation.

The other important dosimetric features and detailed reconstruction of 3D dose distribution are the focus of the follow-up research.

5 Conclusion

In summary, Gd_2O_2S:Eu was successfully synthesized and modified. Then, the composite gel was prepared by incorporating Gd_2O_2S:Eu@PEG into the polyacrylamide-based hydrogel. TEM, DLS, FT-IR, TGA, and spectrofluorometer were used to determine the chemical structure, micromorphology, and optical performance of the composite gel. In addition, the relation of light intensity and the tube current was also studied. During irradiation, radioluminescence of the composite gel can be generated immediately *in situ*, which is able to reduce errors and

measure X-ray doses without any postirradiation waiting time. There is a good linear relationship between the light intensity emitted by the composite gel and the radiation dose (tube current). This study provides a new promising phantom material for 3D gel dosimeter and promotes the safe and effective use of radiotherapy.

Funding information: The present study was supported by the Science and Technology Project of Nantong City (JC2019145), and the Doctoral Scientific Research Foundation of Affiliated Hospital of Nantong University (Tdb19013).

Author contributions: Tao Yang: methodology, writing – review, and editing, funding acquisition; Junhui Wang: writing – original draft, data curation, formal analysis; Jiali Tu: methodology, writing – original draft; Xiaoxi Zhou: resources, formal analysis; Jiamin Sun: formal analysis, investigation; Jian Chen: methodology, resources; Wanxin Wen: supervision, project administration; Yanfei Wang: writing – review and editing, validation;

Conflict of interest: The authors state no conflict of interest.

References

(1) Sung H, Jacques F, Siegel RL, Laversanne M, Soerjomataram I, Jemal A, et al. Global cancer statistics 2020: GLOBOCAN estimates of incidence and mortality worldwide for 36 cancers in 185 countries. CA-Cancer J Clin. 2021; 1–41. doi: 10.3322/caac.21660. Epub ahead of print.

(2) Stewart BW, Wild CP. World cancer report 2014, 6.3 Health systems strengthening for cancer control. Geneva, Switzerland: International Agency for Research on Cancer, World Health Organization; 2014.

(3) Day MJ, Stein G. Chemical effects of ionizing radiation in some gels. Nature. 1950;166(4212):146–7.

(4) Farhood B, Geraily G, Abtahi SMM. A systematic review of clinical applications of polymer gel dosimeters in radiotherapy. Appl Radiat Isotopes. 2019;143:47–59. doi: 10.1016/j.apradiso.2018.08.018.

(5) Baldock C, Harris PJ, Piercy AR, Healy B. Experimental determination of the diffusion coefficient in two-dimensions in ferrous sulphate gels using the finite element method. Australas Phys Eng Sci Med. 2001;24(1):19–30. doi: 10.1007/BF03178282.

(6) Baldock C, Karger CP, Zaidi H. Gel dosimetry provides the optimal end-to-end quality assurance dosimetry for MR-linacs. Med Phys. 2020;47(8):3259–62. doi: 10.1002/mp.14239.

(7) Zhang W, Wang KK, Hu XD, Zhang XH, Chang SQ, Zhang HQ. Preparation of $W_1/O/W_2$ emulsion to limit the diffusion of Fe^{3+} in the Fricke gel 3D dosimeter. Polym Adv Technol. 2020;31(10):2127–35. doi: 10.1002/pat.4934.

(8) Lazzaroni S, Liosi GM, Mariani M, Dondi D. An innovative Fe^{3+} selective ligand for fricke-gel dosimeter. Radiat Phys Chem. 2020;171:108733. doi: 10.1016/j.radphyschem.2020.108733.

(9) Mustaqim AS, Yahaya NZ, Razak NNA, Zin H. The dose enhancement of MAGAT gel dosimeter doped with zinc oxide at 6 MV photon beam. Radiat Phys Chem. 2020;172:108739. doi: 10.1016/j.radphyschem.2020.108739.

(10) Hayashi S, Ono K, Fujino K, Ikeda S, Tanaka K. Novel radiochromic gel dosimeter based on a polyvinyl alcohol – Iodide complex. Radiat Meas. 2020;131:106226. doi: 10.1016/j.radmeas.2019.106226.

(11) Watanabe Y, Maeyama T, Mochizuki A, Mizukami S, Hayashi S, Terazaki T, et al. Verification of dose distribution in high-dose-rate brachytherapy using a nanoclay-based radio-fluorogenic gel dosimeter. Phys Med Biol. 2020;65:175008. doi: 10.1088/1361-6560/ab98d2.

(12) Warman JM, Haas MP, Luthjens LH, Denkova AG, Yao T. A radiofluorogenic polymer-gel makes fixed fluorescent images of complex radiation fields. Polymers. 2018;10:685. doi: 10.3390/polym10060685.

(13) Jiang L, Li WX, Nie J, Wang RS, Chen XJ, Fan WH, et al. Fluorescent nanogel sensors for x-ray dosimetry. ACS Sens. 2021;6(4):1643–8. doi: 10.1021/acssensors.1c00204.

(14) Ivanov RA, Korsakov IE, Formanovskii AA, Paramonov SE, Kuz'mina NP, Kaul' AR. Heteroligand lanthanide dialkyldithiocarbamate complexes with 1,10-phenanthroline: a new approach to synthesis and application for the preparation of sulfides. Russ J Coord Chem+. 2002;28(9):670–2. doi: 10.1023/A:1020051318801.

(15) Ai FR, Goel S, Zhan YH, Valdovinos HF, Chen F, Barnhart TE, et al. Intrinsically ^{89}Zr-labeled Gd_2O_2S:Eu nanophosphors with high *in vivo* stability for dual-modality imaging. Am J Transl Res. 2016;8(12): 5591–600.

(16) Zhao F, Gao S. Pyrolysis of single molecular precursor for monodisperse lanthanide sulfide/oxysulfide nanocrystals. J Mater Chem. 2008;18:949–53. doi: 10.1039/B713636F.

(17) Zhao F, Yuan M, Zhang W, Gao S. Monodisperse lanthanide oxysulfide nanocrystals. J Am Chem Soc. 2006;128(36):11758–9. doi: 10.1021/ja0638410.

(18) Zhang YH, Ai FR, Chen F, Valdovinos HF, Orbay H, Sun HY, et al. Intrinsically zirconium-89 labeled gd_2o_2s:eu nanoprobes for in vivo positron emission tomography and gamma-ray-induced radioluminescence imaging. Small. 2016;12(21):2872–6. doi: 10.1002/smll.201600594.

(19) Boyer JC, Vetrone F, Cuccia LA, Capobianco JA. Synthesis of colloidal upconverting $NaYF_4$ nanocrystals doped with Er^{3+}, Yb^{3+} and Tm^{3+}, Yb^{3+} via thermal decomposition of lanthanide trifluoroacetate precursors. J Am Chem Soc. 2006;128(23):7444–5. doi: 10.1021/ja061848b.

(20) Yan ZQ, Wang F, Wen ZY, Zhan CY, Feng LL, Liu Y, et al. LyP-1-conjugated PEGylated liposomes: a carrier system for targeted therapy of lymphatic metastatic tumor. J Control Rel. 2012;157(1):118–25. doi: 10.1016/j.jconrel.2011.07.034.

(21) Mohamed MS, Veeranarayanan S, Baliyan A, Poulose AC, Nagaoka Y, Minegishi H, et al. Structurally distinct hybrid polymer/lipid nanoconstructs harboring a type-I ribotoxin as cellular imaging and glioblastoma-directed therapeutic

vectors. Macromol Biosci. 2014;14(12):1696–711. doi: 10.1002/mabi.201400248.
(22) Larquet C. Nanoparticles of lanthanide and transition metal oxysulfides: from colloidal synthesis to structure, surface, optical and magnetic properties [PhD dissertation]. Paris (FRA): Sorbonne University; 2018.
(23) Ren F, Liu H, Zhang H, Jiang Z, Xia B, Genevois C, et al. Engineering NIR-IIb fluorescence of Er-based lanthanide nanoparticles for through-skull targeted imaging and imaging-guided surgery of orthotopic glioma. Nano Today. 2020;34:100905. doi: 10.1016/j.nantod.2020.100905.
(24) Goulet M, Rilling M, Gingras L, Beddar S, Beaulieu L, Archambault L. Novel, full 3D scintillation dosimetry using a static plenoptic camera. Med Phys. 2014;41(8):082101. doi: 10.1118/1.4884036.
(25) Sun P, Fu YC, Jiang B. Research progress and application of gel dosimeter in radiotherapy dose verification. Chin J Radiat Oncol (Chin). 2013;22(5):424–6.